A comparison of observations in the tropical western Pacific from ground-based and satellite millimeter-wavelength cloud radars

Zheng Liu,[1] Roger Marchand,[2] and Thomas Ackerman[1]

Received 5 December 2009; revised 30 June 2010; accepted 9 August 2010; published 17 December 2010.

[1] Millimeter-wavelength cloud radar (MMCR) can provide information on the vertical structure of cloud fields and thereby improve our understanding of the spatial distribution of clouds and their role in the climate system. Here we consider the representativeness of ground-based vertically pointing MMCR observations, which have been used in numerous climate studies. MMCR cloud statistics collected at Darwin, Australia, are compared against CloudSat (spaceborne) observations gathered in the near vicinity of the ground site. Overall, the total cloud occurrence vertical profiles observed by CloudSat and the ground-based MMCR agree on a spatial scale of 4° × 4°, although CloudSat is found to observe more high reflectivity cloud than the ground-based MMCR. Computed radar reflectivity using idealized atmospheric profiles suggests that rain (especially below the melting level) influences the observed reflectivities, and this appears to account for much of the differences in the observed distributions of radar reflectivity. After removal of precipitation profiles, CloudSat and ground-based MMCR observations show reasonable agreement. Sampling uncertainty in the CloudSat observations makes comparison at smaller region spatial scales (e.g., 2.5°) difficult and unfeasible for analysis at the time scale of months. Comparison of CloudSat observations with the ground-based data on scales of 4° and 7.5° works well. Comparison of total cloud occurrence and reflectivity distribution of nonprecipitating cloud from the MMCR and CloudSat at spatial scales from 4° to 7.5° show good agreement. This suggests that the properties of the nonprecipitating cloud are relatively homogeneous at this large scale.

Citation: Liu, Z., R. Marchand, and T. Ackerman (2010), A comparison of observations in the tropical western Pacific from ground-based and satellite millimeter-wavelength cloud radars, *J. Geophys. Res.*, *115*, D24206, doi:10.1029/2009JD013575.

1. Introduction

[2] Cloud feedback has been identified as a major source of uncertainty in climate studies, including simulations of both the past century and the current century, particularly studies of climate change over this century [*Solomon et al.*, 2007, and references therein]. To improve the understanding of cloud processes and cloud feedbacks and constrain model uncertainty, long-term global observations of clouds on various scales are desired [*Wielicki et al.*, 1995a]. Global cloud data are often obtained by passive remote sensors on satellites, and these data are used to retrieve cloud properties, for example, by the International Satellite Cloud Climatology Project (ISCCP) [*Schiffer and Rossow*, 1983] and by the Cloud and Earth's Radiant Energy System (CERES) [*Wielicki et al.*, 1995b] Project. However, passive radiances respond to all clouds in the atmospheric column and contain only limited information about the vertical distribution of clouds. Since the vertical radiative heating and the induced circulation on various scales can vary significantly due to changes in the vertical distribution of clouds [*Randall et al.*, 1989; *Slingo and Slingo*, 1991; *Wang and Rossow*, 1998], direct measurements of cloud vertical profiles are desired.

[3] Ground-based millimeter-wavelength cloud radar [*Kollias et al.*, 2007] has proven to be an effective active remote sensing instrument for cloud study over the last decade. Cloud property retrievals [e.g., *Sassen and Liao*, 1996; *Frisch et al.*, 2002; *Mace et al.*, 2002] and radiative impacts [e.g., *McFarlane et al.*, 2007] based on profile measurements from vertically pointing ground-based cloud radar have been proposed and implemented. Their potential for model evaluation is promising as demonstrated in a number of studies [e.g., *Hogan et al.*, 2001a; *McFarlane et al.*, 2007]. These studies generally assume a conversion between temporal statistics and spatial statistics. The model cloud properties are usually instantaneous spatial averages over the area of model resolution, on the scale of tens to hundreds of kilometers. A vertically pointing ground-based cloud radar, however, documents time series of hydrometeor reflectivity in the vertical atmospheric column directly overhead and its horizontal

[1]Department of Atmospheric Sciences, University of Washington, Seattle, Washington, USA.
[2]Joint Institute for the Study of the Atmosphere and Ocean, University of Washington, Seattle, Washington, USA.

0148-0227/10/2009JD013575

field of view is of the order of tens of meters. The temporal statistics of local observations by ground-based instruments are conventionally used to approximate the statistics in a larger area, for example, the size of a GCM grid box. In realistic applications, the validity of this approximation may depend on the meteorological conditions within the region of interest [*Long and Ackerman*, 1995].

[4] CloudSat [*Stephens et al.*, 2002], which was launched into space in 2006, carries on board the first spaceborne cloud radar. Similar to a ground-based cloud radar, the nadir looking cloud profiling radar also samples the cloud vertical profile along the path of its radar signal. In addition to the difference in viewing geometry, sampling strategy is another important distinction between CloudSat and the ground-based cloud radar. Instead of recording the temporal evolution of a local cloud profile, CloudSat records cloud profiles in the vertical cross section of atmosphere beneath the satellite orbit. Because it only takes about 1 min for CloudSat to pass over a domain the size of a typical GCM grid cell, the observations within the GCM grid cell can be treated as a snapshot of the cloud vertical distribution along the CloudSat ground track transects in this grid cell. Although CloudSat has a lower temporal and spatial sampling frequency in a given region, it does provide a direct sampling of the spatial variability of this area compared to the temporal sampling of the ground-based cloud radar.

[5] The basic similarity of CloudSat and the ground-based cloud radar observations coupled with their different viewing geometry and sampling allows us to obtain insight into the characteristics of both sets of observations and explore their application to model evaluation and other climate studies.

[6] There have been several studies comparing CloudSat and ground-based cloud radar observations. *Zuidema and Mapes* [2008] analyzed the cloud vertical structure observed by CloudSat and ship-based cloud radars (35 GHz) over the Bay of Bengal and eastern tropical Pacific. Their studies showed both CloudSat and ship-based cloud radars observed some differences between these two regions, for example, more clouds between 9 and 14 km in the Bay of Bengal than in the tropical eastern Pacific. But there were also some differences not shared by these two radars, and they concluded that point sampling of a few weeks might not serve as a solid representation of a region as large as 10° × 10° longitude/latitude as was used in their study. *Protat et al.* [2009] compared CloudSat observations with ground-based cloud radar observations obtained from five ground-based sites. Their analysis of the mean reflectivity and other basic cloud properties, such as cloud top/base height and the reflectivity distribution, showed generally good agreements between CloudSat and the ground-based cloud radars.

[7] In this study, we focus our analysis of the cloud vertical structures on the tropical western Pacific (TWP) because of its scientific importance and available observations. The tropical western Pacific is an important region in the climate system due to strong solar heating, warm sea surface temperature, and active convection. Our research takes advantage of the MMCRs [*Moran et al.*, 1997] deployed by the U.S. Department of Energy Atmospheric Radiation Measurement (ARM) Program [*Ackerman and Stokes*, 2003]. In this paper, we use MMCR to refer specifically to the ARM ground radars. The ARM Program had an MMCR and other climate research facilities deployed in this region for over a decade [*Mather et al.*, 1998]. Despite considerable progress in our understanding of the cloud distribution and radiative forcing in this region [e.g., *Jakob and Tselioudis*, 2003; *Mather et al.*, 2007; *McFarlane et al.*, 2007], a better understanding of cloud distribution and physical processes is still required for models to produce a more realistic climatology in this region [*Khairoutdinov et al.*, 2005]. Here we compare the observed vertical structure of cloud occurrence and reflectivity distributions from CloudSat and the ground-based MMCR in the TWP region on different spatial scales.

[8] Section 2 describes the data sets used in this study and the comparison scheme. The comparison of observed cloud statistics from CloudSat and the ARM MMCR are shown in section 3 along with an analysis of the factors contributing to the discrepancies.

2. Data and Comparison Scheme

[9] The MMCR is one of the key instruments of this study. The ARM Program installed its first MMCR at the South Great Plains site in late 1996 and later at its other sites at the north slope of Alaska and the tropical western Pacific (TWP). The ARM MMCR is a vertically pointing Doppler radar operating at 35 GHz (8.6 mm wavelength), which is sensitive to hydrometeors including cloud particles and precipitation. The MMCR operates at four routine modes (general, boundary layer, cirrus, and precipitation) with different firmware characteristics to achieve different sensitivities and height resolutions [*Clothiaux et al.*, 1999]. The MMCR reports radar reflectivity approximately every 10 s up to 20 km aboveground level, with a sensitivity from −32 to −48 dBZ at a range of 5 km and a vertical resolution of 45 m below 5 km and 90 m above. The ARM program combines data from the four MMCR modes and other active remote sensors (micropulse lidar, ceilometer) to produce an objective determination of hydrometeor height distributions and a best estimate of their radar reflectivity using the Active Remote Sensing of Clouds (ARSCL) [*Clothiaux et al.*, 2000] algorithm.

[10] There are three ARM TWP sites: Darwin, Manus Island, and Nauru Island. During our analysis of these data for the period overlapping with CloudSat, we found that the radar data at these three sites all have problems to some extent. During 2006–2007, the transmitted power of the Manus MMCR declined from its nominal value of 120–10 W (about 11 dB) by the time it was fixed (Kevin Widener, personal correspondence, 0000). The radar reflectivity observations at Nauru are suffering from problems with the precipitation mode firmware and the ARSCL processing. Because of the hardware and software issues with Manus and Nauru MMCR observations, we focus only on Darwin in this study.

[11] The MMCR at Darwin operates well, but there are some problems with the ARSCL merging process, which produces an artificial sudden increase of reflectivity around 3 km in precipitation. To explore the scope of this problem, we compared the ARSCL radar reflectivity best estimates with the radar reflectivity best estimates compiled by Cloudnet [*Illingworth et al.*, 2007]. Cloudnet is a research project supported by European Commission to provide systematic evaluation of clouds in the forecast models. They proposed an independent algorithm to produce best estimates of radar reflectivity and cloud mask and also processed the

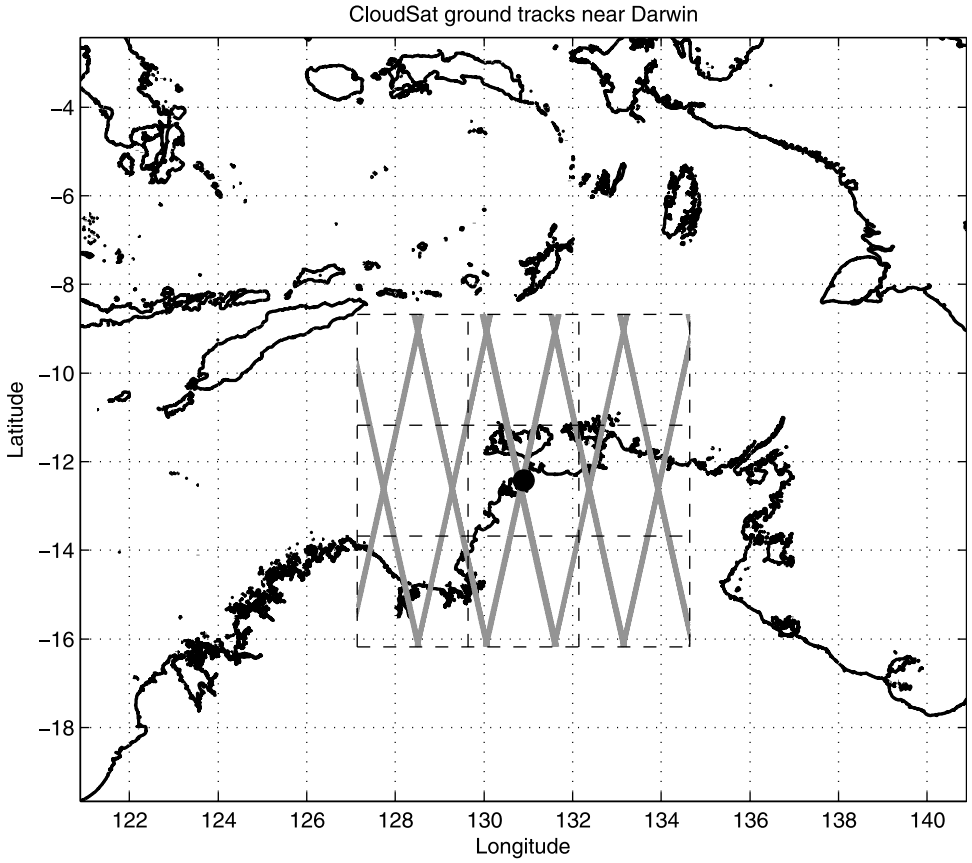

Figure 1. Map of the ARM tropical western Pacific site at Darwin, Australia (black circle). The ground tracks of CloudSat overpasses are shown by gray lines, and the dashed lines mark the boundaries of CloudSat grid box array defined in section 2.

same MMCR data at Darwin. In the tropics, MMCR profiles with reflectivity higher than 0 dBZ below the melting level are usually associated with rainfall. Using this criterion and the surface rain gauge measurements, we classified all profiles as "precipitating" or "nonprecipitating." For nonprecipitating vertical profiles, both the instantaneous reflectivity and cloud statistics of these two data sets are almost identical. For profiles in precipitation, they agree well above the melting level. Our conclusion is that we can still use the ARSCL data set in our analysis except for observations in precipitation below the melting level.

[12] Darwin (12.425°S, 130.891°E) is located on the top end of the Northern Territory of Australia and is under the influence of the Australian summer monsoon [*Drosdowsky*, 1996] with a distinctive wet season and dry season. The wet season onset occurs around December and brings in substantial convection and rainfall. During the wet season, Darwin experiences strong convective activity. On the Tiwi Islands to the north of Darwin, some of the world's deepest convection is observed at this time of year. The monsoon retreats around April and then the dry season lasts for about 6 months into November, with almost no precipitation and very few clouds.

[13] CloudSat is equipped with a 94 GHz nadir looking cloud profiling radar (CPR), which measures backscattered power profiles from hydrometeors along its path with a minimum detectable threshold of about −30 dBZ [*Tanelli et al.*, 2008]. CloudSat has a resolution of about 1.4 km cross track and 1.7 km along track. Its vertical resolution is 480 m but is over-sampled to 240 m in its products. CloudSat's nadir footprint on the surface follows a web of ground tracks (gray lines in Figure 1). Note that the areas between the web tracks are never sampled. CloudSat completes about 14.6 orbits per day and the pattern of its ground track repeats every 16 days with a longitudinal distance between the adjacent web nodes of 1.545° (about 155 km) at the equator. The location of the Darwin site (black dot in Figure 1) is close to one of the nodes on the web, so in every 16 days, CloudSat overflies Darwin twice, once along the descending branch at about 0136 local solar time and once along the ascending branch at about 1351 local solar time. Because CloudSat can only record cloud information along the web track, we define a region around the surface site and use the observed profiles within this region to approximate the cloud statistics for the grid box. In this study, we choose a box of size 2.5° × 2.5°, which is roughly the size of a GCM grid box, and a grid of 3 × 3 boxes centered on the Darwin site (Figure 1). Larger boxes (4° and 7.5°) centered over Darwin are also used to study the changes with spatial scale and the sampling uncertainty.

[14] CloudSat 2B-GEOPROF version 4.0 products provide radar reflectivity and a corresponding cloud mask in each height bin throughout the vertical profiles up to 25 km. A cloud mask threshold of 30 is applied for cloud detection. The data set is available from May 2006 until now. We

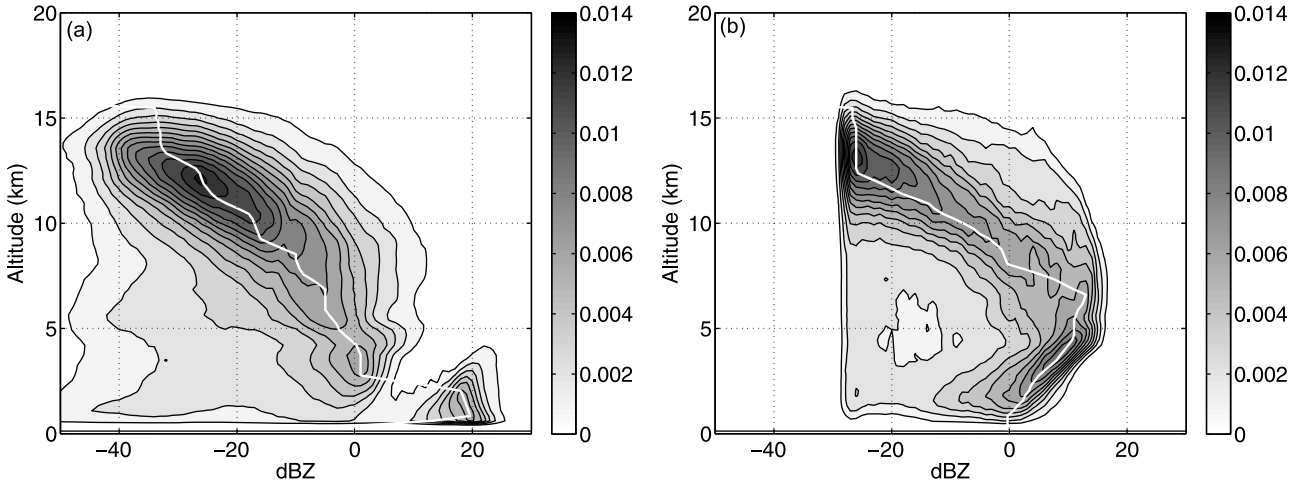

Figure 2. Joint histograms for the Darwin 2006–2007 wet season for (a) the ARM MMCR and (b) the CloudSat nine-box total. The white line indicates the reflectivity value with maximum frequency of occurrence at each level.

focus here on the 2006–2007 wet season and briefly discuss the effects of adding another wet season afterward. Here we use wet season as a term to describe the rainy period at Darwin from December to April.

[15] Other data sets used in this study include optical rain gauge observations, balloon sounding observations of temperature, moisture, and pressure from the ARM site, and the Tropical Rainfall Measuring Mission (TRMM) Multisatellite Precipitation Analysis (TMPA) product 3B43. TMPA 3B43 is an estimate of monthly mean precipitation rate with 0.25° × 0.25° resolution. The two major sources of input to TMPA [*Huffman et al.*, 2007] include the precipitation-related data collected by a variety of passive microwave sensors on low-Earth-orbit satellites (e.g., the TRMM Microwave Imager on TRMM, Advanced Microwave Scanning Radiometer-Earth Observing System on Aqua, etc.), and the window channel (about 10.7 μm) infrared data collected by geosynchronous Earth orbit satellites. The TRMM precipitation radar data are used as a source of calibration, and several sets of surface rain gauge analysis data are incorporated in the final product.

3. Analysis and Results

3.1. Overview

[16] A convenient way to illustrate radar statistics is a joint histogram of radar reflectivity and cloud occurrence. Figure 2a shows the joint histogram observed by the ARM MMCR at Darwin. The frequency distribution of hydrometeor detections falling within a given radar reflectivity interval is computed at every level and plotted together in reflectivity-height coordinates. The normalization includes clear profiles although they are not shown in the joint histograms; consequently, the integration from the minimal detection threshold at any particular altitude gives the radar-derived total cloud occurrence (the ratio of the number of cloudy observations to the total number of observations) at that level. The frequency value within a given reflectivity interval represents the cloud occurrence for hydrometeors within this interval, a cloud macrophysical property, while the shape and position of the frequency distribution in reflectivity space at a given level contains information about cloud microphysical properties.

[17] Above the melting level (about 5 km), both the ARM MMCR and CloudSat have a ridge of contours that is tilted from low reflectivity at higher altitude to high reflectivity at lower altitude, which is consistent with the growth of particles due to collision, aggregation, and the increase in available water vapor for depositional growth as they fall through the atmosphere. In the joint histograms of the ARM MMCR, the tilt of the ridge is more slanted above 10 km than between 5 and 10 km, which may indicate a faster fractional growth rate at higher levels than those between 5 and 10 km or a difference in cloud generation processes at higher levels. Similarly, CloudSat has an increase of slope around 8 km. From 5 to 8 km the CloudSat joint histograms contours are almost vertical with the most frequent occurring reflectivity as high as 13 dBZ. This mode of high reflectivity above the melting layer may be suggestive of large snow/ice particles generated by the intense convection. Non-Rayleigh scattering effects of large ice particles and multiple scattering enhancement [*Battaglia et al.*, 2007] may also contribute to the high reflectivity between 5 and 8 km.

[18] In spite of these similar features, CloudSat observes higher reflectivity at high levels than does the ARM MMCR. The change of most frequently occurring reflectivity with height can be used to show this difference (white lines in Figure 2). They are quite close in value at about 13 km, and both increase in reflectivity at lower levels. However, the increase is more rapid for CloudSat, such that the difference in the location of peak between CloudSat and the ARM MMCR increases from 2 dBZ at 13 km to 18 dBZ at 6 km.

[19] Both physical and statistical factors may contribute to these differences. Because of the different viewing perspectives, spaceborne and ground-based radar signals undergo different attenuation scenarios even when going through the same atmospheric column. Cloud radars operating at wavelength of 3–8 mm undergo significant attenuation in heavy precipitation [*Lhermitte*, 1990]. When we use CloudSat and the MMCR to observe the same precipitating clouds, the radar

reflectivity of clouds above the rain layer observed by the MMCR is significantly underestimated due to the attenuation through the rain layer. However, CloudSat observations are not affected by this issue. As is shown in section 3.2, the difference in reflectivity caused by differential attenuation can be as large as 17 dB. Besides differential attenuation, differences in radar frequency and beam width further complicated this issue.

[20] Sampling uncertainty of CloudSat observations is another important factor. CloudSat observations are sampled along its ground tracks. When we infer cloud statistics from observations along its ground track transects, there is uncertainty associated with the relative position of these transects to the clouds. The importance of this factor in the interpretation of the comparison of CloudSat and the MMCR observations is also explored in detail in section 3.3.

[21] For the ARM MMCR, the cloud occurrence between −40 and −30 dBZ exhibits a typical trimodal structure [*Johnson et al.*, 1999] with maxima around 1, 5, and 13 km. The lowest and the highest modes correspond to boundary layer cumulus and high level cirrus, respectively. The mid-level peak may be related to the cumulus congestus outflow at the stable layer associated with the melting level [*Johnson et al.*, 1996]. The trimodal structure of low reflectivity clouds is not directly observed by CloudSat likely due to the lower sensitivity of CloudSat, especially in the lowest 1 km, where ground clutter [*Marchand et al.*, 2008] significantly reduces radar sensitivity near the surface. Even in the ARM MMCR joint histograms, this trimodal structure only shows up in the range of low reflectivity. If clouds with a full range of reflectivities are considered, convective activities associated with high reflectivity are still the major phenomenon during the wet season at Darwin. Convection is so intense during the wet season that radar-detected cloud tops frequently reach 16 km and higher.

[22] Below the melting level, precipitation dominates in both the ARM MMCR and CloudSat observations. The reflectivity sharp increase around 3 km in the ARM joint histograms related to the artifact of the ARSCL processing problem. The CloudSat observed reflectivity decreases rapidly from about 5 km to surface. Because of the relatively shorter wavelength (3.2 mm) of the 94 GHz cloud radar, compared with the ARM MMCR, liquid water and water vapor attenuation is stronger. The gaseous attenuation for the ARM MMCR is usually only fractions of 1 dB [*Matrosov et al.*, 2004] and is often neglected.

[23] The enhancement of the reflectivity at the melting level, or the "brightband" observed by CloudSat, is not as evident as one would observe from a precipitation radar. *Sassen et al.* [2005] investigated the melting level and associated brightband using ground-based lidar and radars at 9.6, 35, and 94 GHz. They found that the reflectivity increase of the melting particles is not followed by a decrease of reflectivity at the base of the melting level in the ground-based 94 GHz radar observations. This is likely due to the non-Rayleigh scattering occurring at this short wavelength [*Kollias and Albrecht*, 2005]. However, the CloudSat observations do show a weak brightband near 4.6 km due to the attenuation in rain below the melting level [*Sassen et al.*, 2007]. This weak reflectivity enhancement is accentuated by an evident "dark band" at the upper melting layer, with a decrease of reflectivity of about 5 dB. The exact mechanism for the dark band is not clear, but it is thought to be associated with the non-Rayleigh backscattering reduction for the slightly melted snow particles [*Sassen et al.*, 2007].

3.2. Rain Attenuation

[24] CloudSat reflectivity profiles often show significant surface clutter within the lowest several range gates due to strong surface reflection, but sometimes the surface clutter is missing because the attenuation is so strong that the signal cannot even reach the surface. Reflectivity below −10 dBZ in the lowest 1–2 km is usually associated with drizzle in the ARM MMCR observations, but for CloudSat, these cases may actually be heavy precipitation with large droplets and large water content. If the reflectivity values at these levels are not considered in the context of reflectivity at levels above and adjacent observations, the interpretation of heavy precipitation as light drizzle may have a significant impact on cloud property retrievals and associated radiative heating, latent heating and water budget calculations. In this case, the decrease of reflectivity between the melting level and the ground level is a result of the path integrated attenuation through the precipitation layer rather than actual changes in the cloud microphysics. Similarly, for the ARM MMCR, the reflectivity of clouds above rain is underestimated due to attenuation and the reduced effective range and sensitivity.

[25] Attenuation of the radar signal occurs as a result of two processes, scattering and absorption of the energy by the scatterer. Under the Rayleigh scattering approximation, the scattering cross section is much smaller than the absorption cross section, so the contribution of scattering to attenuation is negligible. When the particle size parameter $\chi = \pi D/\lambda$ gets close to 1 (characteristic diameter of $D = 0.5$ mm at 94 GHz and 2.7 mm at 35 GHz), the scattering cross section and the absorption cross section are of equal importance in terms of extinction. Because of its shorter wavelength, CloudSat is more attenuated in rain than the ARM MMCR.

[26] During the 2006–2007 wet season at Darwin, precipitation events are frequent. Using the precipitation identification criterion we introduced earlier, we find that throughout this period the occurrence of cloud below 5 km is 41% and the occurrence of rain is 13% out of the total number of MMCR observations. Nearly one out of three profiles with cloud below 5 km is associated with rain. For the 2007–2008 wet season, the rain to cloud ratio is slightly higher than one third. Consequently, the effect of the attenuation on radar signals is an important factor in characterizing the observed cloud statistics.

[27] To illustrate the effects of heavy rain, we computed the radar reflectivity profiles from an idealized rainy column using CloudSat and ARM MMCR configurations, Mie scattering theory, and the assumption of single scattering. Our idealized profile has rain from the surface to 5 km and ice cloud aloft up to 10 km. A uniform liquid water content profile of 0.5 g m^{-3} and an effective diameter of 1 mm are assumed for the rain layer. The ice cloud above is assumed to have a uniform ice water content of 0.05 g m^{-3} and an effective diameter of 0.1 mm. Both the liquid and ice particles are assumed to obey gamma size distributions. No mixed phase cloud is considered in this calculation. The sounding profile above cloud top (10 km) uses the average sounding data measured at the ARM Darwin site from December 2006

to April 2007, and below cloud top the atmosphere is assumed to be saturated. We choose a hydrometeor profile with both large particles and large water content in order to investigate the extent of the effects of precipitation on the radar reflectivity profiles of the ARM MMCR and CloudSat.

[28] The idealized radar reflectivity decreases dramatically when traveling through the rain layer with an attenuation rate of 13.4 dB/km at 94 GHz and 3.4 dB/km at 35 GHz. Because of the relatively small number of direct CloudSat overpasses and the difference in the field of view (kilometers versus tens of meters) between CloudSat and the ARM MMCR, it is difficult to find collocated reflectivity profiles similar to our simulation. But we do find individual profiles showing similar features. For profiles of thick stratiform precipitation observed by CloudSat, a decrease of reflectivity from over 15 dBZ at 5 km to below −15 dBZ near the surface is frequently seen and in the ARM MMCR observations, a 5–10 dB loss of reflectivity through a rain layer is usual.

[29] In addition to the differing radar frequencies, different viewing geometries can also contribute to the differences in the observed cloud statistics. Attenuation through the ice cloud is negligible compared with the attenuation in the rain layer below due to their difference in index of refraction, so the power loss of the radar signal for the 94 GHz radar observing from space is much less than it is for the upward looking 35 GHz radar above 5 km. Because of the path integrated attenuation of the 35 GHz radar, the calculated radar reflectivity of the ice layer above rain at 35 GHz viewing upward is 17.2 dB lower than at 94 GHz viewing downward. The gaseous attenuation difference of the two radars above the melting level is less than 1 dB above the melting level and increases quickly toward the surface to values as large as 6.3 dB. Therefore the differential attenuation of the radars with different viewing geometries is the primary cause for the reflectivity difference for clouds over rain in our idealized profile and plausibly explains the shift in peak reflectivity position above the melting level in Figure 2.

[30] The idealized radar profile reproduces the key features of the differences in cloud statistics observed from CloudSat and the ARM MMCR although the rates of attenuation and values of attenuation in the idealization are not the same as observed. The observations cover a range of conditions, while the simulated radar reflectivity profiles are calculated from one prescribed atmospheric profile. The actual value of attenuation through a particular rain layer varies with the rainwater content and the rain droplet size distribution. Multiple scattering can also play an important role in the observed reflectivity difference because CloudSat has a much wider signal beam within the troposphere than the ARM MMCR. *Battaglia et al.* [2007] studied the effects of multiple scattering of radar signals in a CloudSat configuration using a Monte Carlo-based simulator with cloud profiles extracted from Cloud Resolving Models (CRM) for midlatitude mesoscale systems. They demonstrated that the multiple scattering enhancement (difference of radar reflectivity between a single-scattering configuration and a multiple-scattering configuration) at lower levels is highly correlated with ice particles above. Because of the large field of view of CloudSat, the multiple scattering effect is especially significant. Attenuation in precipitation is compensated for by the scattering enhancement to the beam from more than 20 dB/km to less than 10 dB/km. The value of the reflectivity enhancement in heavy precipitation can be as large as 79 dB near the surface. Multiple scattering enhancement is a possible mechanism to partially account for the differences between our simulation and CloudSat observations.

3.3. Sampling Uncertainty Analysis

[31] When comparing two statistical results, it is important to assess the statistical significance of the differences that may be found. Because the ARM MMCR continuously documents profiles of vertical hydrometeor distribution with a time step of 10 s, the large sample size ensures that its sampling uncertainty is much smaller than the sampling uncertainty of CloudSat. Conventionally, estimation of sampling uncertainty requires the assumption of a sampling distribution. CloudSat samples the clouds within a given region along one transect at a time. The observations within the same overpass are strongly correlated, but samples in different overpass are almost independent of each other. Consequently, the number of independent samples within a prescribed area is much less than the number of samples (profiles) and is related to the decorrelation scale of the clouds along an overpass transect. Thus neither a Gaussian distribution nor an independent sampling assumption is valid for CloudSat observations. The "moving-block" bootstrap resampling [*Wilks*, 1997] method is a more acceptable technique for statistical analysis in this case. The idea of the bootstrap method is to simulate the sampling process from the original population by sampling from an approximate distribution, which in most practical cases is the empirical distribution of observed data. A bootstrap resampling technique approximates the uncertainty of cloud occurrence from a large number of "replications" of the original CloudSat data set, i.e., the CloudSat observations in the region of interest. Each replication is composed of observations randomly sampled from the original data set. To preserve the spatial correlation within a CloudSat overpass, a number of consecutive observations are sampled together instead of only one profile at a time. This group of consecutive observations is called a "moving block," and the number of consecutive observations is called the "block length." It is assumed that with a proper block length and a large enough set of replications, the distribution of the CloudSat sampling statistics can be approximated by the sampling distribution of the replications.

[32] Because CloudSat cloud occurrence is estimated from transects of observations within the region of interest, the sampling uncertainty of this kind of estimate is related to the cloudiness of the region. There is less ambiguity when the region of interest is cloud free or totally cloud filled because the transect is cloud free or totally cloud filled no matter how the transect is taken across the region. We expect the uncertainty to increase when the region is partly cloudy because the cloud statistics estimated from the transect observations may depend on the orientation and position of the transects within the region. This is potentially a serious problem for CloudSat observations in the convective tropics with its high frequency of broken cloud fields.

[33] *van de Poll et al.* [2006] studied the sampling uncertainty of cloud fraction estimates from random transect observations using synthetic data resembling observations of the spaceborne NASA-LITE lidar mission. Their analysis

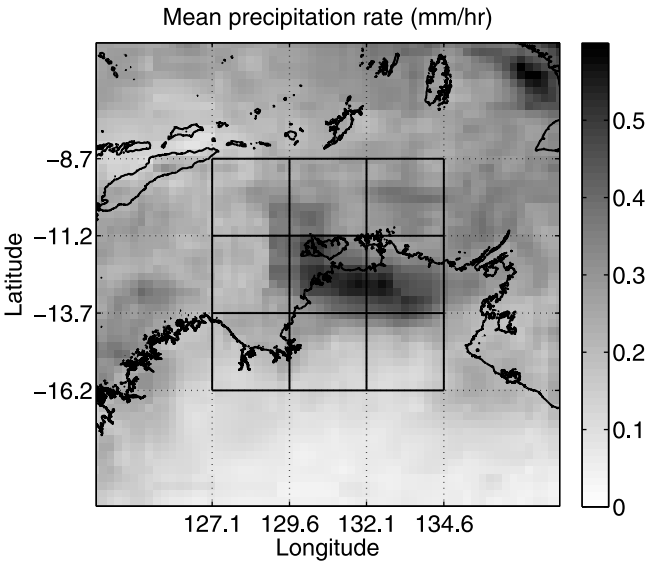

Figure 3. Mean precipitation rate from TRMM 3B43 data during the 2006–2007 wet season. The solid black lines mark the boundaries of the CloudSat grid box array defined in section 2.

took the width of the 90% confidence interval of the cloud fraction distribution as a proxy to evaluate the sampling uncertainty and estimated the true cloud fraction using a Bayesian inference approach. The level of uncertainty reaches a maximum when the true cloud fraction is 50% and decreases to zero when approaching completely clear or 100% cloudy conditions, according to their simulation.

[34] The nine 2.5° CloudSat boxes that we use here (see Figure 1) extend through a variety of terrain conditions from ocean, to continental inland, which may suggest variability in cloud statistics within the nine boxes. Figure 3 shows the TMPA mean precipitation rate near Darwin during the 2006–2007 wet season with the nine CloudSat boxes in the center. Because the TMPA precipitation estimates rely heavily on microwave and IR data in addition to precipitation radar data, they will likely have much less sampling uncertainty than CloudSat when averaged over a calendar month, even with a resolution of 0.25°. The two inland boxes, the southern and southeastern boxes, are dry while the central and eastern boxes are wettest. Since the differences in precipitation patterns among the nine boxes are observed, we expect the nine boxes to have different cloud statistics.

[35] Vertical profiles of cloud occurrence of the nine CloudSat boxes and the ARM MMCR are presented in Figure 4. Without the consideration of sampling uncertainty, these cloud occurrence profiles seem to be related to the topography and precipitation pattern. For example, the three boxes on the west side (red) have very similar cloud occurrence at all levels, which may be attributed to their oceanic properties. The central box has considerably more clouds than the other boxes at all levels, which agrees with the TRMM precipitation records. The relatively lower cloud occurrence in the northern box and the southern box also corresponds to the drier condition shown in Figure 3. The southeastern box is the most inland box and has lower clouds than the other boxes. The question is whether the consideration of the sampling uncertainty still allows us to conclude the similarity between the precipitation and cloud occurrence pattern is genuine.

[36] The size of our CloudSat grid box is 2.5° and the distance between adjacent CloudSat ground tracks is about 1.55°. So on average, a 2.5° box includes three ground tracks. CloudSat repeats the same ground track only once in every 16 days or 24 times a year. For an average 2.5° grid box, there are only 72 overpasses a year. For locales like Darwin, where only about 5 months (wet season) are of interest, the number goes down to about 30. Table 1 lists the number of complete transects in each CloudSat box. By complete transect, we mean that the transect covers most of the box length from north to south; overpasses near the corners of the CloudSat boxes are not considered. During the 2006–2007 wet season, the number of transects in each of the nine CloudSat boxes ranges from 16 to 37, each with a length of about 280 km. *van de Poll et al.* [2006] simulated the level of uncertainty for 450 km long transects with a true cloud fraction of 50% and produced an uncertainty of about 0.15 for 16 transects and 0.1 for 30 transects. Because the sampling uncertainty maximizes at a true cloud fraction of 50%, these values give the maximum sampling uncertainty for cloud fraction estimated from transect observations using a given level of confidence. With the same sampling statistics and number of transects, if we choose a higher level of confidence (to be more conservative), the width of the confidence interval is relaxed to a larger value, hence higher sampling uncertainty is estimated. In our analysis we use a higher level of confidence of 95% and a shorter transect length, so we expect the estimated sampling uncertainty to be somewhat larger than 0.15.

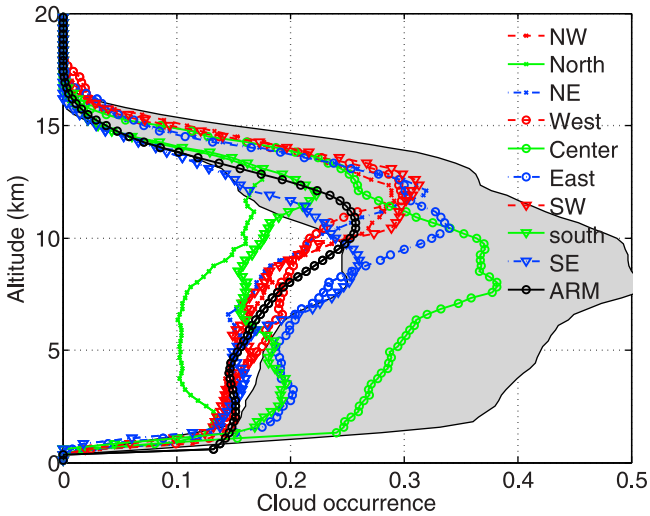

Figure 4. Comparison of vertical profiles of cloud occurrence for the nine CloudSat boxes defined in section 2 and the ARM MMCR observations. Boxes along the same longitude line are plotted with the same color, and boxes along the same latitude line are plotted with the same symbol. The ARM MMCR cloud occurrence (truncated at −30 dBZ) is plotted with black circles. The shaded region indicates the 95% confidence interval for the central box.

Table 1. The Number of CloudSat Transects (Each Containing a Minimum of 50 Profiles), the Total Number of Profiles, and the Ratio of Profiles With Precipitation to the Total Number of Profiles in the Nine 2.5° × 2.5° Boxes During the 2006–2007 Wet Season

Box Position	NW	North	NE	West	Center	East	SW	South	SE
Number of transects	27	35	27	37	16	36	27	35	27
Number of profiles	6009	8871	6380	9582	4144	8956	6681	8577	6690
Precipitation ratio	0.122	0.091	0.127	0.129	0.243	0.161	0.111	0.147	0.126

[37] According to the discussion above, despite the similarity between the precipitation pattern (Figure 3) and the cloud occurrence pattern (Figure 4), we cannot support the distinction of the cloud occurrence pattern and its connection with the precipitation pattern, because of the large sampling uncertainty. The shaded region in Figure 4 shows the 95% confidence interval of the CloudSat cloud occurrence profile for the central box. From below 2 km to over 13 km, the sampling uncertainty (the width of the confidence interval) is as large as 0.2, compared with a total cloud occurrence of less than 40%. On the scale of 2.5°, the sampling uncertainty is so large that the spatial variability cannot be statistically resolved. This is particularly discouraging given that our data set is one complete wet season.

[38] As seen in Figure 4, the sampling uncertainty increases as cloud occurrence increase because the maximum cloud occurrence at any level is smaller than 50%. Another message from Figure 4 is that the sampling uncertainty is an important factor for the interpretation of the statistics of cloud properties and radiative impacts derived from CloudSat and CALIPSO observations. It is especially significant when the spatial scale is relatively small (2.5°). The sampling uncertainty for the cloud occurrence of the central box (width of the shaded region in Figure 4) reaches 0.2 or about ±0.1 for a total cloud fraction of 30%.

[39] This uncertainty propagates from the original observations to the retrievals based on these observations. For example, the mean radiative heating rates derived from CloudSat/CALIPSO observations at a 2.5° scale suffer the same level of sampling uncertainty, even if the mean heating rates are averaged from profile-by-profile retrievals. Since the CloudSat sampling uncertainty is so large on this scale, one must carefully consider it before claiming physical conclusions from CloudSat data. In some applications, the same cautions apply to CALIPSO.

[40] One expects that the level of uncertainty can be reduced if more observations are included, either by adding another year of data or by using a larger grid box to construct the statistics. At best, the uncertainty should reduce inversely with the square root of the number of independent samples. So two seasons will at most reduce the uncertainty by 30%; however, this does not consider interannual variability [e.g., *Holland*, 1986; *Drosdowsky*, 1996] which can be significant. We applied our same analysis to the 2007–2008 wet season and the average of the two wet seasons (results not shown). It turns out that adding another 5 month season of data provides only a marginal improvement in sampling uncertainty.

[41] An alternative way to increase the number of independent observations is to use a larger grid box. It is actually more effective to double the size of the domain than to add another year of data. When doubling the size of the box, the number of ground tracks inside the box doubles or triples, increasing from two to four ground tracks to six to eight tracks, depending on where the center of the box is. At the same time, the length of ground tracks also doubles and longer transects of observations can also help to reduce the sampling uncertainty. This is illustrated in section 3.4 with the consideration of potentially greater spatial variability when a larger grid box is used for the analysis.

3.4. Effects of Precipitation and Spatial Scale on Observations

[42] To evaluate the effects of precipitation, we identified radar profiles with a possibility of precipitation using similar criteria to those used earlier for the comparison of ARSCL and Cloudnet observations. From the ARM MMCR mode data, we find that during rain events the radar reflectivity is usually greater than 0 dBZ between the surface and 5 km. Therefore we define a profile as a precipitation profile when a reflectivity value greater than 0 dBZ is detected in any range gate below 5 km or when a rain rate larger than 0.1 mm/h is measured by a surface rain gauge. MMCR profiles obtained within 10 min following rain gauge rain records are also classified as precipitating to reduce the effect of wet radome attenuation [*Hogan et al.*, 2001b]. For CloudSat profiles, we also identify all profiles with reflectivity greater than 0 dBZ below 5 km as precipitating. Under these criteria, 14% of the total MMCR profiles at Darwin are precipitating; for CloudSat this ratio is 24%, 16%, and 13%, respectively, for the 2.5°, 4.0°, and 7.5° boxes centered over Darwin. The decrease of this ratio with increasing spatial scale is likely due to the large sampling uncertainty in the 2.5° box. As we show later, the occurrence of precipitating clouds is not sensitive to the changes in spatial scale up to 7.5°.

[43] Because of the attenuation of the MMCR signal through the precipitation layer, the MMCR reflectivity of cloud above precipitation is underestimated, sometimes even dropping below the minimum detectable threshold. If the radar reflectivity is underestimated but still above the minimum detectable threshold, high-reflectivity cloud is registered as low-reflectivity cloud without changing the total cloud occurrence at the corresponding level. In this case, the shape of the distribution is changed, but total cloud occurrence at this level is conserved. Otherwise the total cloud occurrence also decreases. In reality, both situations may happen and attenuation may produce differences in both the total cloud occurrence (as defined by any radar signal greater than -30 dBZ) and the shape of the distribution between CloudSat and the ARM MMCR.

[44] Vertical profiles of the total cloud occurrence from all profiles and from profiles after the removal of precipitation are shown in Figure 5. The sampling uncertainty is shown as the shaded region. To conform with CloudSat's sensitivity, the observations for the ARM MMCR are truncated at −30 dBZ. On the scale of 2.5°, CloudSat observes considerably more clouds at almost all levels relative to the

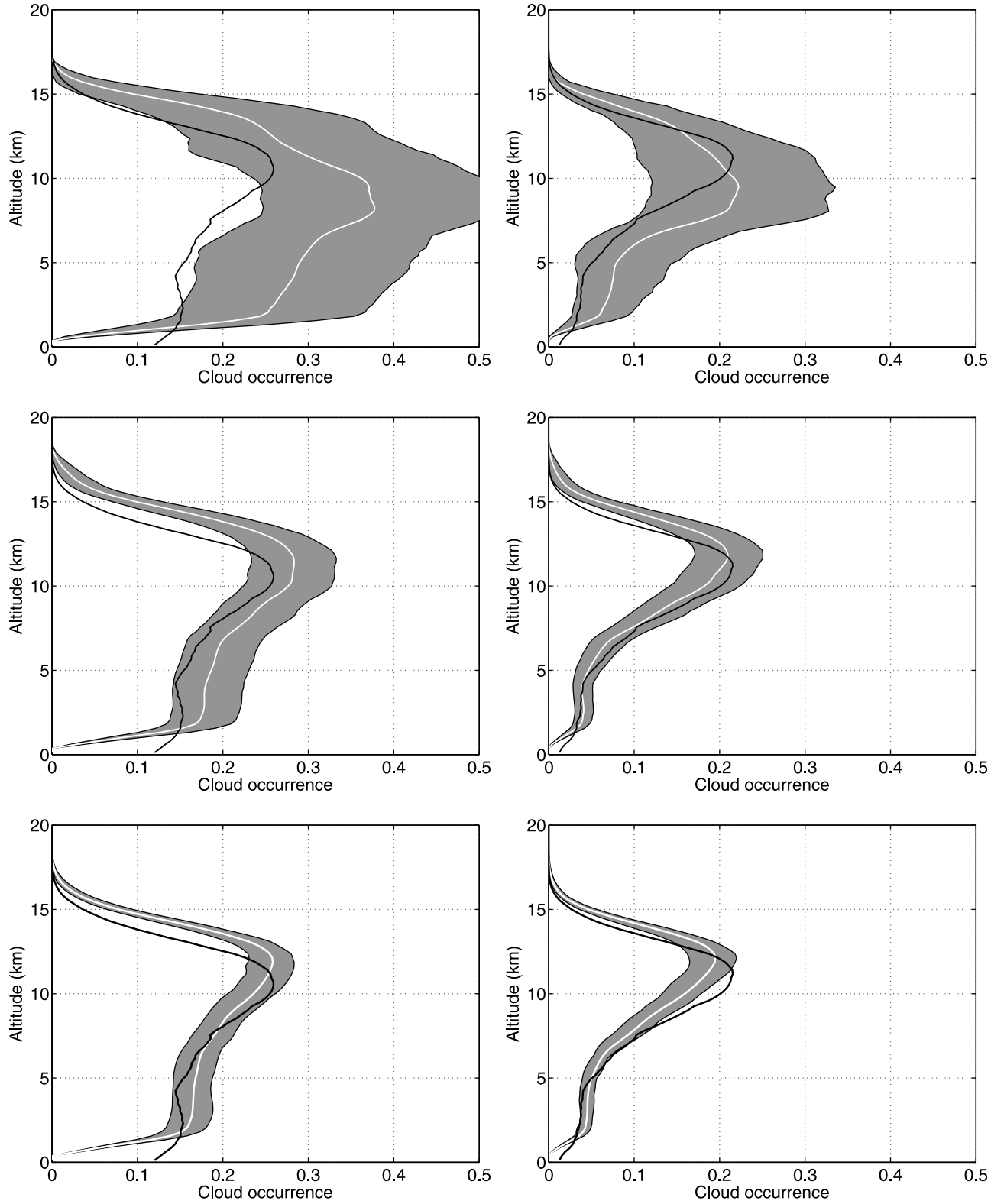

Figure 5. Comparison of CloudSat total cloud occurrence based on (top) 2.5°, (middle) 4.0°, and (bottom) 7.5° boxes centered over Darwin for (left) all profiles and (right) profiles without precipitation. The black lines are the cloud occurrence (truncated at −30 dBZ) of the ARM MMCR truncated. The white line is cloud occurrence of the CloudSat central box. The shaded region shows the 95% confidence interval.

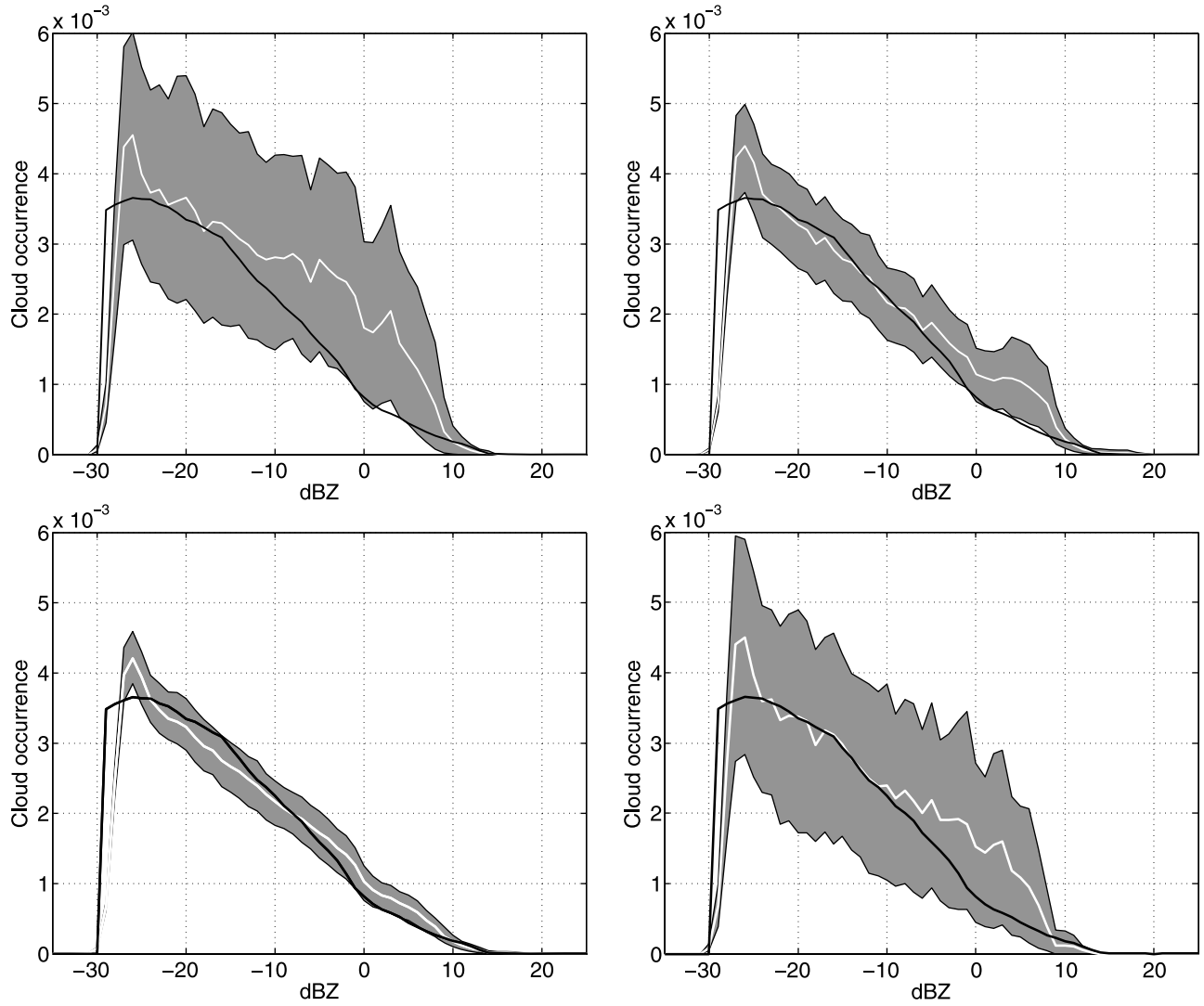

Figure 6. Column overall reflectivity distribution summed from the surface to 18 km without precipitation for the MMCR (black line) and (top left) the CloudSat central box, (top right) a 4° × 4° box center over Darwin site, (bottom left) sum of all the nine boxes around Darwin, and (bottom right) the central box shifted north by 0.25°. The shaded regions are the bootstrapped 95% confidence intervals.

ARM MMCR when precipitation is not removed. This difference is statistically significant at the 95% confidence level. After the removal of precipitation, the two come into a decent agreement, although the level of uncertainty is still high. We note that due to the removal of the precipitating profiles, the autocorrelation between adjacent profiles is reduced. The resulting level of uncertainty estimated by the moving-block bootstrap method for this broken record is likely overly optimistic (i.e., the actual uncertainty is larger).

[45] On the scale of 4°, CloudSat observes significantly more high cloud above 12 km than the ARM MMCR. Below 12 km, the ARM MMCR still observes fewer clouds at almost all levels but its total cloud occurrence profile now fits within the 95% confidence interval of the CloudSat observations even before the removal of precipitation. This agreement holds when we use a 7.5° grid box (all of the nine 2.5° boxes). The consistent agreement suggests that the differential attenuation caused by precipitation does not introduce dramatic differences in vertical total cloud occurrence profiles observed by the ARM MMCR and CloudSat. Therefore the fact that significant differences occur between the vertical cloud occurrence profiles observed by the ARM MMCR and by CloudSat in the 2.5° box probably indicates that the CloudSat observations along the two ground tracks within that box are statistically insufficient to represent the cloud statistics of the whole box. We expect the two observations would agree on 2.5° scale if the clouds within this box were properly sampled by CloudSat. Although the differential attenuation does not introduce significant differences to vertical profiles of total cloud occurrence observed from CloudSat and ARM MMCR, it changes the distribution of cloud occurrence among the reflectivity ranges as is shown in Figure 2. We compute the overall reflectivity distribution from the surface to 18 km for profiles without precipitation (Figure 6). The overall reflectivity distribution of the nonprecipitating profiles observed by CloudSat and the ARM MMCR agree on all three spatial scales, which leads us to

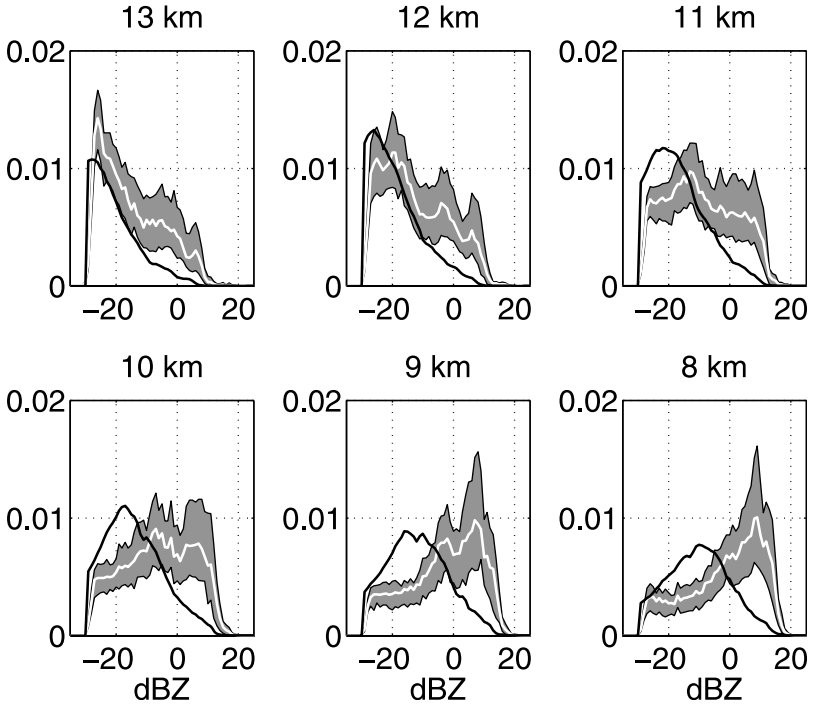

Figure 7. Comparison of frequency distributions of the ARM MMCR (black line) and a CloudSat 4° box (white line) centered over Darwin. The shaded region around the CloudSat distribution is the 95% confidence interval calculated with the moving-block bootstrap method.

conclude that differential attenuation in precipitation is a major cause of the difference seen in Figure 2.

[46] One would assume that in the 7.5° area around Darwin, the complicated ocean/land boundaries should increase the variability of the domain averaged cloud statistics rather than decrease the variability (see Figure 3), compared with the 2.5° box. On the other hand, in a larger area, not only does the level of sampling uncertainty decrease as the number of observations increase, but also the statistics calculated with the observations along the CloudSat ground tracks have a better spatial sampling of the domain and are more representative of the cloud statistics of the whole area. As the size of the CloudSat grid box increases from 2.5° to 4° and 7.5° (Figure 5), not only does the level of uncertainty decrease as the number of observations increase, but also the agreement between CloudSat and the ARM MMCR is improved. This suggests that the total cloud occurrence around Darwin is not sensitive to a change in spatial scale up to 7.5° and the increased spatial variability is insignificant relative to the sampling uncertainty. The nonprecipitating cloud occurrence profile of the 2.5° box (Figure 5) does agree with the results from larger boxes and the ARM MMCR. This indicates that the nonprecipitating cloud occurrence is less likely to be biased by sampling patterns even with a 2.5° box. It is probably due to the relatively more uniform spatial distribution of nonprecipitating clouds and hence lower sensitivity to the change in spatial scale compared with precipitating clouds.

[47] According to Figure 2, the most frequently observed reflectivity at any level above 7 km decreases with altitude and this decrease holds for nonprecipitating clouds as well (not shown). So the increase of cloud occurrence with decreasing reflectivity in Figure 6 can also be interpreted as an increase of nonprecipitating cloud occurrence with height, which agrees with the observed nonprecipitating cloud occurrence vertical profiles (Figure 5).

[48] Figure 6 also shows consistent agreement of the overall reflectivity distribution observed by the ARM MMCR and CloudSat as the spatial scale increase, which is suggestive of the low sensitivity of the reflectivity distribution with spatial scale. Note that the precipitation pattern (Figure 3) around Darwin demonstrates high sensitivity to spatial scale. However, the cloud occurrence of all clouds, the cloud occurrence of nonprecipitating clouds, and the reflectivity distribution of nonprecipitating clouds are not sensitive to spatial scale. It is probably the variability in the cloud microphysics of the precipitating clouds that produces to the spatial variability of precipitation within the region shown in Figure 3.

[49] In the preceding discussion, we used the overall reflectivity distribution to evaluate the agreement between CloudSat and the ARM MMCR. It is also useful to examine the reflectivity distribution at different altitudes to obtain information about the cloud statistics which may not be evident in the vertical integral. Figure 7 shows the comparison of cloud occurrence distributions with respect to radar reflectivity between the CloudSat central box and the ARM MMCR from 13 to 8 km. At the levels of 13 km and 12 km, CloudSat and the ARM MMCR cloud occurrence distribution agree well at the low reflectivity end (−25 to −15 dBZ). CloudSat has a second peak in cloud occurrence at a higher reflectivity (−5 to 5 dBZ), where the ARM MMCR reports little clouds. Below 11 km, the most frequently observed clouds by the ARM MMCR have reflectiv-

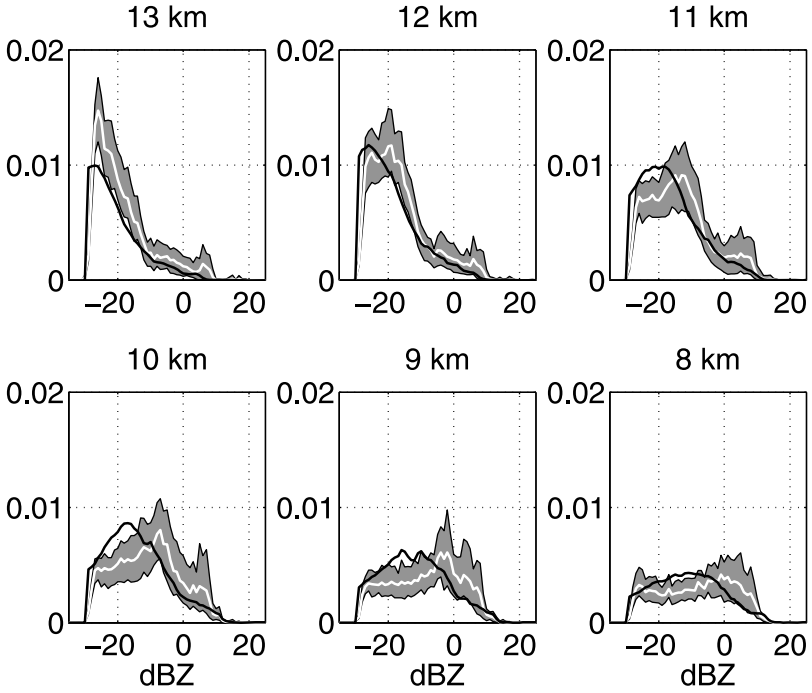

Figure 8. Comparison of frequency distributions of the ARM MMCR (black line) and a CloudSat 4° box (white line) centered over Darwin using profiles without precipitation. The shaded region around the CloudSat distribution is the 95% confidence interval calculated with the moving-block bootstrap method.

ities around −20 dBZ, while for CloudSat the most frequently observed clouds have reflectivities ranging from 0 to 10 dBZ, although the total cloud occurrence (total area under the curves) is similar for both.

[50] The cloud occurrence of CloudSat and the ARM MMCR without precipitation is shown in Figure 8. Above 11 km, CloudSat and the ARM MMCR are in good agreement at all reflectivity values. From 10 to 8 km, the cloud occurrence values above–5 dBZ agree well. However, the differences between CloudSat and MMCR cloud occurrence near −20 dBZ remain significant. We are not sure what the cause of this inconsistency is but speculate that the different horizontal and vertical resolution of CloudSat and the ARM MMCR observations may be a factor. For example, the weakly reflecting cloud detected by the MMCR at −20 dBZ may not fill enough of the CloudSat beam to be detected. Overall, the improvement in the agreement between CloudSat and the ARM MMCR statistics after precipitation removal confirms our assumption that the differential attenuation of the cloud radar signal in precipitation is the primary cause of the different cloud statistics presented in Figure 7.

[51] One partial reason for the good agreement between the CloudSat and the ARM MMCR overall reflectivity distributions at larger scales is the compensation between different levels (Figure 8). For example, CloudSat observes more cloud at −20 dBZ at 13 km, while the MMCR observes more cloud at −20 dBZ at 10 km. The differences of cloud occurrence at −20 dBZ at these two levels almost compensate for each other when we take the vertical sum. Again, we speculate that this may be a result of the differences in the horizontal and vertical resolution of these two radars, a topic that will need further study.

[52] We also considered the response of CloudSat and the MMCR observations to the diurnal cycle. We subset CloudSat observations by daytime overpass and nighttime overpass and choose the ARM MMCR observations around CloudSat overpasses with a time window of 2, 4, and 6 h. Although there are differences between daytime overpasses and nighttime overpasses, the conclusions of our current analysis about the agreement between the ARM MMCR and CloudSat observations are not affected.

4. Conclusions

[53] CloudSat provides us with global cloud structure observations and motivates us to study the statistical consistency of cloud radar observations at a point (ground-based radar) and in an area around it (spaceborne radar) in order to investigate the statistical basis for model evaluation using ground-based cloud radar profiles and retrieved cloud properties from these profiles. Our analysis of observed cloud statistics at the three ARM TWP sites showed that all three MMCRs have problems to some extent during the period of our interest. Only the Darwin radar is working properly, although its ARSCL reflectivity estimates are problematic in rain. In our experience, these problems have not been adequately documented in the quality reports in the ARM data archive, so potential users should exercise great care when using the ARM MMCR data.

[54] During the 2006–2007 wet season at Darwin, the ARM MMCR and CloudSat document significantly different cloud statistics illustrated by the joint histograms of radar reflectivity and cloud occurrence. Above the melting level, CloudSat reports much higher reflectivity than the ARM

MMCR. Below the melting level, CloudSat suffers strong attenuation in rain, and its reflectivity decreases as the altitude decreases. This latter effect is due to the path-integrated attenuation rather than physical changes in cloud properties. The observed differences are produced by both physical (rain attenuation) and statistical (sampling uncertainty) issues. Different responses of the MMCR and CloudSat to non-Rayleigh scattering particles and multiple scattering enhancement of CloudSat signals can also contribute to the differences. After we do a first-order removal of precipitation profiles by removing profiles with a reflectivity greater than 0 dBZ below the melting level (which is typically associated with rain), CloudSat and ARM MMCR cloud occurrences agree within the 95% confidence interval.

[55] Because the precipitation layer can significantly modify the reflectivity distribution and detection of cloud above the rain layer and the modification is affected by factors such as droplet size, rain rate/rainwater content, and geometric thickness of the raining layer, one should be careful when using the MMCR observations in rain and the associated retrieval properties of high-level clouds in these profiles.

[56] The sampling uncertainty of CloudSat observations was evaluated using a "moving-block" bootstrap resampling method. Moving-block bootstrapping can capture the contribution of data autocorrelation to variability in the cloud occurrence. Because of the strong autocorrelation of data within a given CloudSat transect, individual profiles can not be treated as independent data. During the 5 month period we studied, CloudSat does not have a sufficient number of overpasses at the 2.5° scale to undertake an analysis of spatial variability due to the large sampling uncertainty. Either a larger grid box or a longer time period can be used to lower the sampling uncertainty but at the expense of introducing spatial variability and interannual variability, which will also increase the uncertainty level. Our analysis using both the 2006–2007 and the 2007–2008 wet seasons shows only marginally improvement of sampling uncertainty at the 2.5° scale likely due to the introduction of interannual variability.

[57] As we increase the size of the CloudSat sampling box, the vertical profiles of total cloud occurrence from CloudSat on the scale of 4° and 7.5° agree with the ARM MMCR observations, while significant differences remain at a scale of 2.5° scale. We conclude, first, that CloudSat observations along only two ground tracks within the 2.5° box are insufficient to represent of the cloud statistics within the box; second, with respect to cloud occurrence, attenuation in precipitation does not cause significant differences between the ARM MMCR and CloudSat observations at the 7.5° scale; and third, total cloud occurrence around Darwin is not very sensitive to changes in spatial scale up to 7.5°.

[58] CloudSat and ARM MMCR overall reflectivity distributions for nonprecipitating clouds continue to show agreement within the 95% confidence level at larger spatial scale, even as the estimated uncertainty decreases. Within an area as large as 7.5° around Darwin, the spatial variability for nonprecipitating clouds is expected to be larger than in a 2.5° box, given the complicated surface conditions. A possible explanation for the agreement between regional averaged statistics and localized statistics is that the nonprecipitating clouds are relatively uniformly distributed over a large area, resulting in statistics that are not particularly sensitive to spatial scale, and it is the precipitating clouds that are responsible for the variability of cloud statistics. The fact that the total cloud occurrence for all clouds is not sensitive to the changes in spatial scale implies the spatial variability of cloud microphysical properties of precipitating clouds is probably responsible for the variation of the precipitation in this region.

[59] Our analysis supports the use of ground-based MMCR observations for model comparison on scales of 5°–10° around the observation site and temporal scales of a few months or more. We also show that nadir viewing satellite data analyses are very sensitive to spatial scale due to the large autocorrelation in the samples. The combined observations from ground and satellite radars, however, provide a detailed prospective on cloud property statistics unavailable from any other instruments and are critical to our understanding of clouds and comparison with models.

[60] **Acknowledgments.** This work greatly benefited from discussions with Kevin Widener and Eugene Clothiaux about the issues associated with the ground-based MMCR. We also benefited from discussions with Alain Protat regarding CloudSat sampling and Darwin radar data analysis of the Cloudnet group. We thank Ewan O'Connor for his kindly help to process the Cloudnet version of the ARM MMCR data. The authors also thank Robert Wood and Qiang Fu for their comments on the original manuscript. This research was supported by Department of Energy Atmospheric Radiation Measurement Program through award 39189 from Pacific Northwest National Laboratory.

References

Ackerman, T. P., and G. M. Stokes (2003), The Atmospheric Radiation Measurement program, *Phys. Today*, *43*, 38–44.

Battaglia, A., M. O. Ajewole, and C. Simmer (2007), Evaluation of radar multiple scattering effects in Cloudsat configuration, *Atmos. Chem. Phys.*, *7*, 1719–1730.

Clothiaux, E., et al. (1999), The Atmospheric Radiation Measurement program cloud radars: Operational modes, *J. Atmos. Oceanic. Technol.*, *16*, 819–827.

Clothiaux, E., T. Ackerman, G. Mace, K. Moran, R. Marchand, M. Miller, and B. E. Martner (2000), Objective determination of cloud heights and radar reflectivities using a combination of active remote sensors at the ARM CART sites, *J. Appl. Meteorol.*, *39*, 645–665.

Drosdowsky, W. (1996), Variability of the Australian summer monsoon at Darwin: 1957–1992, *J. Clim.*, *9*, 85–96.

Frisch, S., M. Shupe, I. Djalalova, G. Feingold, and M. Poellot (2002), The retrieval of stratus cloud droplet effective radius with cloud radars, *J. Atmos. Oceanic. Technol.*, *19*(6), 835–842.

Hogan, R., C. Jacob, and A. Illingworth (2001a), Comparison of ECMWF winter-season cloud fraction with radar-derived values, *J. Appl. Meteorol.*, *40*, 513–525.

Hogan, R., D. Bounoil, D. Ladd, E. J. O'Connor, and A. J. Illingworth (2001b), Absolute calibration of 94/95-GHz radars using rain, *J. Atmos. Oceanic. Technol.*, *20*, 572–580.

Holland, G. J. (1986), Interannual variability of the Australian summer monsoon at Darwin: 1952–82, *Mon. Weather Rev.*, *114*, 594–604.

Huffman, G. J., et al. (2007), The TRMM multisatellite precipitation analysis: Quasi-global, multiyear, combined-sensor precipitation estimates at fine scale, *J. Hydrometeorol.*, *8*, 38–55.

Illingworth, A. J., et al. (2007), Cloudnet, *Bull. Am. Meteorol. Soc.*, *88*, 883–898.

Jakob, C., and G. Tselioudis (2003), Objective identification of cloud regimes in the tropical western Pacific, *Geophys. Res. Lett.*, *30*(21), 2082, doi:10.1029/2003GL018367.

Johnson, R. H., P. E. Ciesielski, and K. A. Hart (1996), Tropical inversions near the 0°C level, *J. Atmos. Sci.*, *53*(13), 1838–1855.

Johnson, R. H., T. M. Rickenbach, S. Rutledge, P. E. Ciesielski, and W. H. Schubert (1999), Trimodal characteristics of tropical convection, *J. Clim.*, *12*, 2397–2418.

Khairoutdinov, M. F., D. A. Randall, and C. DeMott (2005), Simulations of the atmospheric general circulation using a cloud-resolving model as a superparameterization of physical process, *J. Atmos. Sci.*, *62*, 2136–2154.

Kollias, P., and B. Albrecht (2005), Why the melting layer radar reflectivity is not bright at 94 GHz, *Geophys. Res. Lett.*, *32*, L24818, doi:10.1029/2005GL024074.

Kollias, P., E. Clothiaux, M. Miller, B. Albrecht, G. Stephens, and T. Ackerman (2007), Millimeter-wavelength radars: New frontier in atmospheric cloud and precipitation research, *Bull. Am. Meteorol. Soc.*, *80*, 1608–1624.

Lhermitte, R. (1990), Attenuation and scattering of millimeter wavelength radiation by clouds and precipitation, *J. Atmos. Oceanic. Technol.*, *7*, 464–479.

Long, C., and T. Ackerman (1995), Surface measurements of solar irradiance: A study of the spatial correlation between simultaneous measurements at separated sites, *J. Appl. Meteorol.*, *34*, 1039–1046.

Mace, G., A. Heymsfield, and M. Poellot (2002), On retrieving the microphysical properties of cirrus clouds using the moments of the millimeter-wavelength Doppler spectrum, *J. Geophys. Res.*, *107*(D24), 4815, doi:10.1029/2001JD001308.

Marchand, G., G. Mace, T. Ackerman, and G. Stephens (2008), Hydrometeor detection using CloudSat—An Earth-orbiting 94-GHz cloud radar, *J. Atmos. Oceanic. Technol.*, *25*, 519–533.

Mather, J. H., T. P. Ackerman, W. E. Clements, F. J. Barnes, M. D. Ivey, L. D. Hatfield, and R. M. Reynolds (1998), An atmospheric radiation and cloud station in the tropical western Pacific, *Bull. Am. Meteorol. Soc.*, *79*, 627–642.

Mather, J. H., S. McFarlane, M. Miller, and K. Johnson (2007), Cloud properties and associated radiative heating rates in the tropical western Pacific, *J. Geophys. Res.*, *112*, D05201, doi:10.1029/2006JD007555.

Matrosov, S., T. Uttal, and D. A. Hazen (2004), Evaluation of radar reflectivity-based estimates of water content in stratiform marine clouds, *J. Appl. Meteorol.*, *43*, 405–418.

McFarlane, S., J. Mather, and T. Ackerman (2007), Analysis of tropical radiative heating profiles: A comparison of models and observations, *J. Geophys. Res.*, *112*, D14218, doi:10.1029/2006JD008290.

Moran, K. P., B. E. Martner, M. J. Post, R. A. Kropfli, D. C. Welsh, and K. B. Widener (1997), An unattended cloud-profiling radar for use in climate research, *Bull. Am. Meteorol. Soc.*, *79*(3), 443–455.

Protat, A., et al. (2009), Assessment of CloudSat reflectivity measurements and ice cloud properties using ground-based and airborne cloud radar observations, *J. Atmos. Oceanic Technol.*, *26*, 1717–1741.

Randall, D. A., Harshvardhan, D. Dazlich, and T. G. Corsetti (1989), Interactions among radiation, convection, and large-scale dynamics in a general circulation model, *J. Atmos. Sci.*, *46*, 1943–1970.

Sassen, K., and L. Liao (1996), Estimation of cloud content by w-band radar, *J. Appl. Meteorol.*, *35*(6), 923–938.

Sassen, K., J. R. Campbell, J. Zhu, P. Kollias, M. Shupe, and C. Williams (2005), Lidar and triple-wavelength Doppler radar measurements of the melting layer: A revised model for dark- and brightband phenomena, *J. Appl. Meteorol.*, *44*(3), 301–312.

Sassen, K., S. Matrosov, and J. Campbell (2007), CloudSat spaceborne 94 GHz radar bright bands in the melting layer: An attenuation-driven upside-down lidar analog, *Geophys. Res. Lett.*, *34*, L16818, doi:10.1029/2007GL030291.

Schiffer, R. A., and W. B. Rossow (1983), The International Satellite Cloud Climatology Project (ISCCP): The First Project of the World Climate Research Programme, *Bull. Am. Meteorol. Soc.*, *64*, 779–784

Slingo, A., and J. M. Slingo (1991), The response of a general circulation model to cloud longwave radiative forcing, *Q. J. R. Meteorol. Soc.*, *117*, 333–364.

Solomon, S., D. Qin, M. Manning, Z. Chen, M. Marquis, K. Averyt, M. Tignor, and H. L. Miller (Eds.) (2007), *Climate Change 2007: The Physical Science Basis—Contribution of Working Group I to the Fourth Assessment Report of the Intergovernmental Panel on Climate Change*, 996 pp., Cambridge Univ. Press, Cambridge, U. K.

Stephens, G., et al. (2002), The Cloudsat mission and the A-train, *Bull. Am. Meteorol. Soc.*, *83*, 1771–1790.

Tanelli, S., S. L. Durden, E. Im, K. S. Pak, D. G. Reinke, P. Partain, J. M. Haynes, and R. T. Marchand (2008), CloudSat's cloud profiling radar after 2 years in orbit: Performance, calibration, and processing, *IEEE Trans. Geosci. Remote Sens.*, *46*(11), 3560–3573.

van de Poll, H., H. Grubb, and I. Astin (2006), Sampling uncertainty properties of cloud fraction estimates from random transect observations, *J. Geophys. Res.*, *111*, D22218, doi:10.1029/2006JD007189.

Wang, J., and W. B. Rossow (1998), Effects of cloud vertical structure on atmospheric circulation in the GISS GCM, *J. Clim.*, *11*, 3010–3029.

Wielicki, B. A., R. D. Cess, M. D. King, D. A. Randall, and E. F. Harrison (1995a), Mission to planet Earth: Role of clouds and radiation in climate, *Bull. Am. Meteorol. Soc.*, *76*, 2125–2153.

Wielicki, B. A., B. R. Barkstrom, E. F. Harrison, R. B. Lee III, G. L. Smith, and J. E. Cooper (1995b), Clouds and the Earth's Radiant Energy System (CERES): An Earth observing system experiment, *Bull. Am. Meteorol. Soc.*, *77*, 853–868.

Wilks, D. (1997), Resampling hypothesis tests for autocorrelated fields, *J. Clim.*, *10*, 65–82.

Zuidema, P., and B. Mapes (2008), Cloud vertical structure observed from space and ship over the Bay of Bengal and the eastern tropical Pacific, *J. Meteorol. Soc. Jpn.*, *86A*, 205–218.

T. Ackerman and Z. Liu, Department of Atmospheric Sciences, University of Washington, Seattle, WA 98195, USA.

R. Marchand, Joint Institute for the Study of the Atmosphere and Ocean, University of Washington, Seattle, WA 98195, USA.